Flinders
UNIVERSITY

Archived at the Flinders Academic Commons:
http://dspace.flinders.edu.au/dspace/

The following article appeared as:

Jones, D.B., Bellm, S.M., Blanco, F., Fuss, M., Garcia, G., Limao-Vieira, P. and Brunger, M.J., 2012. Differential cross sections for the electron impact excitation of pyrimidine. Journal of Chemical Physics, 137, 074304.

and may be found at:
http://jcp.aip.org/resource/1/jcpsa6/v137/i7/p074304_s1

DOI: http://dx.doi.org/10.1063/1.4743961

Copyright (2012) American Institute of Physics. This article may be downloaded for personal use only. Any other use requires prior permission of the authors and the American Institute of Physics.

Differential cross sections for the electron impact excitation of pyrimidine

D. B. Jones, S. M. Bellm, F. Blanco, M. Fuss, G. García et al.

Citation: J. Chem. Phys. **137**, 074304 (2012); doi: 10.1063/1.4743961
View online: http://dx.doi.org/10.1063/1.4743961
View Table of Contents: http://jcp.aip.org/resource/1/JCPSA6/v137/i7
Published by the American Institute of Physics.

Additional information on J. Chem. Phys.

Journal Homepage: http://jcp.aip.org/
Journal Information: http://jcp.aip.org/about/about_the_journal
Top downloads: http://jcp.aip.org/features/most_downloaded
Information for Authors: http://jcp.aip.org/authors

ADVERTISEMENT

Downloaded 01 Jan 2013 to 129.96.237.231. Redistribution subject to AIP license or copyright; see http://jcp.aip.org/about/rights_and_permissions

Differential cross sections for the electron impact excitation of pyrimidine

D. B. Jones,[1,a)] S. M. Bellm,[2] F. Blanco,[3] M. Fuss,[4] G. García,[4] P. Limão-Vieira,[5] and M. J. Brunger[2,6,b)]

[1]*School of Chemical and Physical Sciences, Flinders University, GPO Box 2100, Adelaide, SA 5001, Australia*
[2]*ARC Centre for Antimatter-Matter Studies, School of Chemical and Physical Sciences, Flinders University, GPO Box 2100, Adelaide, SA 5001, Australia*
[3]*Departamento de Física Atómica, Molecular y Nuclear, Universidad Complutense de Madrid, Madrid E-28040, Spain*
[4]*Instituto de Física Fundamental, Consejo Superior de Investigaciones Cientificas, Madrid E-28006, Spain*
[5]*Departamento de Física, CEFITEC, Faculdade de Ciências e Tecnologia, Universidade Nova de Lisboa, 2829-516 Caparica, Portugal*
[6]*Institute of Mathematical Sciences, University of Malaya, Kuala Lumpur 50603, Malaysia*

(Received 20 June 2012; accepted 26 July 2012; published online 15 August 2012)

We report on differential cross section (DCS) measurements for the electron-impact excitation of the electronic states of pyrimidine. The energy range of the present measurements was 15–50 eV with the angular range of the measurements being 10°–90°. All measured DCSs displayed forward-peaked angular distributions, consistent with the relatively large magnitudes for the dipole moment and dipole polarizability of pyrimidine. Excitations to triplet states were found to be particularly important in some energy loss features at the lower incident electron energies. To the best of our knowledge there are no other experimental data or theoretical computations against which we can compare the present results. © *2012 American Institute of Physics*. [http://dx.doi.org/10.1063/1.4743961]

I. INTRODUCTION

It has become widely understood that low-energy electrons play an important role in how ionizing radiation deposits its energy in matter.[1] Here ionizing radiation has been found to produce an abundance of low-energy secondary electrons which can efficiently interact with the biological media to deposit their energy. These interactions take place through excitation, ionization, or dissociative electron attachment processes that can alter the biochemistry or induce DNA strand breakage.[2] This may ultimately lead to cellular mutation or necrosis. The importance of understanding these interactions in biological systems has created an urgent demand for low-energy electron-impact collision data. These data are a prerequisite for understanding and modelling radiation induced damage in complex biological systems.[3]

Electron-impact differential cross sections, $\sigma_i(E_0, \theta)$, that describe the probability that an electron with energy E_0 will induce a transition to the ith state and scatter into the θ-direction (with respect to the incident electrons direction) provide the most detail about the electron-target interaction. However, the complexity in performing electron scattering experiments to measure differential cross section (DCS) data for large molecules of biological relevance has made such data scarce. The large size of such molecules also makes the full scale *ab initio* calculations required to accurately model low-energy electron scattering from molecules largely intractable. The limited availability of collision cross sections for low-energy electron interactions with biologically relevant molecules has led to charged-particle track simulations often being evaluated in gaseous or bulk water.[4–6] To further improve models of radiation damage of biological systems it is desirable to include a more accurate description of the biological media that goes beyond water, such as including contributions from DNA analogs. However, this requires an accurate knowledge of the low-energy electron scattering phenomena from the constituent biomolecules. Gas-phase scattering data from biomolecules that are structural analogs to DNA may assist in this regard, with recent experiments revealing that DNA damage resulting from dissociative electron attachment occurs through changes to individual molecular subunits rather than over the entire length.[7,8] Note further that the utility of employing gas-phase collision data to model behaviour in condensed matter has been recently demonstrated by White and Robson.[9] With the paucity of available experimental and theoretical data for scattering processes from large biomolecules, gas-phase measurements will provide an ideal testing ground for the further development and assessment of theoretical scattering models.

Pyrimidine ($C_4H_4N_2$) is the primary structure for many larger biological molecules. Specifically, pyrimidine forms the basis for the DNA/RNA bases cytosine, thymine, and uracil. An understanding of electron scattering phenomena for pyrimidine is therefore potentially important for elucidating the origins of electron scattering behaviour in larger biological systems. This has led to a number of recent electron scattering experiments from pyrimidine. These have included low- and intermediate-energy elastic electron scattering experiments,[10,11] measurements of the threshold-electron excitation spectra, intermediate-energy electron energy loss spectra,[3] total cross sections,[12] dynamical and binary triple-differential cross sections,[13,14] and electron energy loss spectra of pyrimidine condensed on thin argon films.[15] Recently,

a)Electronic mail: darryl.jones@flinders.edu.au.
b)Electronic mail: michael.brunger@flinders.edu.au.

 © 2012 American Institute of Physics

Downloaded 01 Jan 2013 to 129.96.237.231. Redistribution subject to AIP license or copyright; see http://jcp.aip.org/about/rights_and_permissions

we have published[16] data for electron-impact excitation of two excitation features of pyrimidine at 15 and 30 eV, in a comparative study with benzene relating to the nature of electron induced π-π^* transitions in aromatic compounds. In this paper, we expand on that earlier work to present the complete set of differential cross sections for electron-impact excitations to the electronic states of pyrimidine up to the first ionization energy at four incident electron energies ranging between 15 and 50 eV. The present paper also follows from our earlier paper[17] where we reported a joint experimental and R-matrix theoretical study on the integral cross sections (ICS) for electron-impact excitations of pyrimidine.

II. PHYSICAL PROPERTIES AND EXCITED ELECTRONIC STATE SPECTROSCOPY OF PYRIMIDINE

Pyrimidine is an azabenzene with two N atoms located at the 1 and 3 positions in the six member ring. It is a symmetric planar molecule having C_{2v} point group symmetry, with a $^1A_1$ ground electronic state. Here the introduction of the N atoms into the aromatic ring creates a permanent dipole moment of 2.28–2.39 D.[18–20] Pyrimidine also has a high dipole polarizability of ~60 a.u.[12] This combination of a large dipole moment and high dipole polarizability has been found to play an important role in the scattering behaviour. In particular, the elastic scattering DCS exhibited strongly forward-peaked angular distributions, with this behaviour being attributed to the strong interaction between the electron and the dipole/dipole polarized target.[10,17] We, therefore, expect this dipole moment and high dipole polarizability to play an important role in the electron-impact discrete excitation processes.

Substantial knowledge of the excited electronic states of pyrimidine has been gained from the measurement of its photo-absorption spectra, which has attracted considerable interest.[3,21–23] In particular, the photo-absorption studies on pyrimidine, in combination with benzene and other azabenzenes,[21] have provided key insights into how the introduction of N atoms into the benzene ring influences the nature of the n-π^* and π-π^* transitions. These experiments have been interpreted with the assistance of numerous theoretical calculations to provide a detailed understanding of the singlet electronic states.[22–26] The pyrimidine photo-absorption spectrum is dominated by three broad features attributed to strong dipole-allowed transitions at 5.2, 6.7, and 7.6 eV. Specifically, the bulk of the intensity observed for these features has been assigned to π-π^* transitions to the $^1B_2$, $^1A_1$, and $^1A_1 + {}^1B_2$ symmetry states, respectively. These features are supplemented by weak dipole-allowed ($^1B_1$) features at ~4.2 and ~6.0 eV. We also note that significant spectral intensity is also observed at 8.2 and 8.9 eV, which is attributed to a complex mixture of Rydberg-like excitations converging to different ion states. These spectral assignments are supported by theoretical calculations based on time-dependent density functional theory[22] and the symmetry-adapted cluster configuration interaction method.[25] This behaviour is similar to that observed in the present electron energy loss spectra (see Fig. 1), where we find six spectral features. However, the present spectra also display substantially different behaviour to that observed for photo-absorption. These differences stem from the absence of strict spin or dipole selection rules to the present electron scattering experiments. In particular, singlet → triplet excitation processes, forbidden in photo-absorption, become accessible in low-energy electron collisions through an exchange interaction. The available data on the singlet → triplet excitation processes is less comprehensive than that for the dipole-allowed transitions, with the weak transitions and complexity of the spectra making assignment difficult. Here only the near-threshold electron energy loss spectra,[23] hot photo-absorption spectra,[24] and theoretical calculations[22–24] have provided a somewhat limited description of the low-lying triplet states. We have recently demonstrated that the electron-impact excitation of pyrimidine to higher lying triplet states may be particularly important at low incident electron energies.[16] We, therefore, follow the state assignments outlined in Masin *et al.*[17] where we reported the most comprehensive coverage yet of transitions to singlet and triplet states.

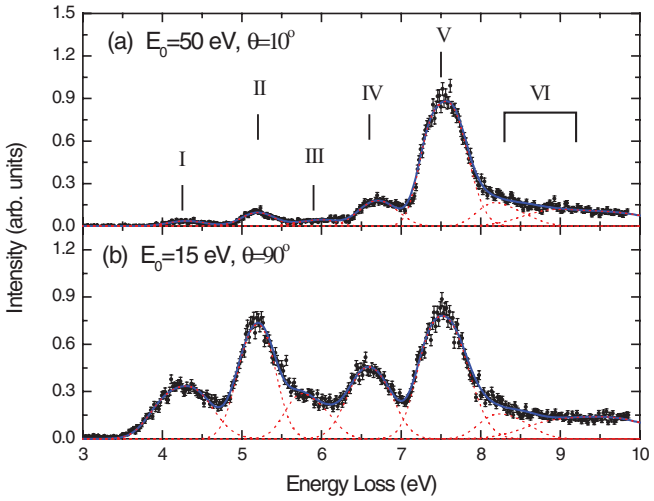

FIG. 1. Typical electron impact energy loss spectra measured for (a) $E_0 = 50$ eV and $\theta = 10°$ and (b) $E_0 = 15$ eV and $\theta = 90°$. For each spectrum, the spectral deconvolutions for each feature (dashed lines) and their sum (solid line) are also presented. Reprinted with permission from Z. Masin *et al.*, J. Chem. Phys. **136**, 144310 (2012). Copyright 2012 American Institute of Physics. See text for full details.

III. EXPERIMENTAL METHOD AND ANALYSIS

Electron energy loss spectra (see Fig. 1) have been measured using an apparatus based at Flinders University. The full details of this apparatus have been described previously by Brunger and Teubner.[27] Briefly, a well-collimated and mono-energetic electron beam is crossed with an orthogonal beam of pyrimidine. Typical electron fluxes were in the range 2–5 nA, as measured in a Faraday cup located after the collision region. Here the pyrimidine sample (Sigma-Aldrich/Austin Chemical Company, >98.9% assay) underwent repeated freeze-pump-thaw cycles to remove any dissolved gases. The pyrimidine effused out of a 0.7 mm i.d. capillary, with the flow rate being controlled by a variable leak valve. In this study the chamber pressure during the experiments was typically in the order of ~5×10^{-6} Torr, to

Downloaded 01 Jan 2013 to 129.96.237.231. Redistribution subject to AIP license or copyright; see http://jcp.aip.org/about/rights_and_permissions

ensure that there were no noticeable effects due to multiple scattering. Electrons scattering into the θ-direction were detected using a channel electron multiplier after passing through a hemispherical energy analyser. Note that the combination of a hemispherical energy-selector and analyser enabled us to obtain an energy resolution of the order of ~65 meV (FWHM) in the present measurements. Here a linear voltage ramp controlled the energy loss value of the detected electrons. This voltage ramp was further synchronized to a multi-channel scaler to record the number of electrons detected at each energy loss value. The present electron energy loss spectra at each incident energy and scattering angle were therefore built up by continually scanning over a range of energy loss values between –0.5 and 9.8 eV. In this way, the sensitivity of the results due to fluctuations in electron beam current and target gas density are minimised. In the present investigation the electron energy loss spectrum at each incident electron energy and scattering angle was measured between 2 and 4 times to ensure reproducibility of the obtained results. Note the interference of the primary electron beam and the physical constraints imposed by the size of the electron analyser and energy selector restrict the present angular measurements to scattering angles between 10° and 90°.

The electron energy loss spectra at each incident electron energy and scattering angle were then deconvolved into contributions arising from a single transition or a group of unresolvable transitions. Here either one or two Gaussian functions were employed as fitting functions for each spectral feature, with the positions and widths of each feature having been established through consideration of the available photo-absorption spectra,[3,21–23] threshold-electron excitation spectra,[23] and theoretical calculations.[22–24] A full discussion of the present spectral assignments has been reported in our earlier paper[17] relating to the ICS, so we do not repeat those details here. At each incident energy and scattering angle, the amplitudes of the Gaussian functions were varied, while keeping the positions and widths fixed, in a least-squares fitting procedure to determine the best overall fit to the spectrum. The area under the fitting functions for an individual or sum of unresolved transitions relates to the intensity of that transition. The intensity ratio (I_i/I_0) of the ith inelastic feature to the elastic transition at each energy and scattering angle can then be related to the DCS for that feature,$\sigma_i(E_0, \theta)$, at that energy and angle:

$$\sigma_i(E_0, \theta) = \frac{I_i}{I_0}\eta_{i0}\sigma_0(E_0, \theta). \quad (1)$$

Here $\sigma_0(E_0, \theta)$ is the elastic DCS for pyrimidine while η_{i0} is the relative transmission efficiency for the inelastically and elastically scattered electrons. Following a procedure similar to that outlined by Allan,[28] an additional focussing lens synchronized to the linear voltage ramp was employed to minimize variations in the detection efficiency for electrons detected with different energy loss values. Here the relative transmission efficiency was determined to be unity to within an uncertainty of 20%. The absolute scale of the inelastic DCSs is set by the recently measured elastic DCS of Palihawadana *et al.*[10] Note that the absolute scale and angular distributions of the experimental data for elastic scattering from pyrimidine were found to be in excellent agreement with sophisticated calculations.[10,17] The uncertainty on the present measurements is obtained by combining the uncertainties of the elastic scattering DCS, the transmission efficiency and the statistical uncertainty of the inelastic scattering intensity ratio at each energy and angle.

IV. RESULTS AND DISCUSSION

In Fig. 1, we present representative electron energy loss spectra at (a) 15 eV and (b) 50 eV. These spectra have been discussed previously in relation to our joint experimental and theoretical study into the pyrimidine ICS for electron-impact excitation,[17] so we only provide a brief description again here. Six prominent and uniquely resolvable spectral features have been observed in the energy loss spectra. Here the sixth feature is comprised of two energy loss features at 8.3 and 9.2 eV. These features are loosely combined due to the complex nature and potential ambiguity in assigning the large number of Rydberg-like excitations that are found in this energy region. The behaviour of all of the spectral features changes significantly for the varying kinematical conditions covered in the present experiments. In spectrum (a), the larger impact energy of 50 eV and the small 10° scattering angle favours dipole-allowed singlet → singlet transitions from direct scattering events. Conversely, in spectrum (b) the low incident electron energy of 15 eV and relatively large 90° scattering angle favours singlet → triplet transitions occurring through an electron-exchange interaction. The large number of accessible and unresolved singlet → singlet and singlet → triplet transitions predicted to lie within each spectral feature makes the characterisation of the individual spectral assignments difficult. However, by studying the behaviour of the DCS for the unresolved transitions in each spectral feature we may understand which transitions play an important role in the scattering phenomena.

The current DCS data for electron-impact excitations in pyrimidine are presented in Tables I–VII. ICS derived from the present DCS using a generalised oscillator strength extrapolation to forward scattering angles that were reported in our earlier study,[17] are also included for completeness. To our knowledge there are currently no available experimental data or theoretical calculations against which we can compare these DCS measurements. Therefore, in order to offer quantitative insights into the behaviour of the electron-impact excitation processes, we compare the DCS behaviour for the unresolved excitations in the different energy loss features. In Fig. 2 we consider the DCS for electron-impact excitations into the unresolved $1^3B_1 + 1^1B_1 + 1^3A_1 + 1^3A_2 + 1^1A_2 + 1^3B_2$ (E_{loss} ~ 4.3 eV) and $2^3B_1 + 2^1A_2 + 2^1B_1$ (E_{loss} ~ 5.9 eV) electronic states. These features are compared as they both give weak contributions to the available photo-absorption spectra. In Fig. 3 we consider the DCS for the electron-impact excitations to the unresolved $2^3A_1 + 1^1B_2 + 2^3A_2$ (E_{loss} ~ 5.2 eV), $2^3B_2 + 2^1A_1 + 2^1B_2 + 3^3A_1 + 3^3B_2$ (E_{loss} ~ 6.7 eV) and $3^1A_1 + 4^1A_1 + 3^1B_2 + 3^1B_1 + 4^1B_2$ (E_{loss} ~ 7.5 eV) electronic states. These features all contain dipole-allowed excitation processes to $^1A_1$ or $^1B_2$ excited states, which produce the dominant peak features

Downloaded 01 Jan 2013 to 129.96.237.231. Redistribution subject to AIP license or copyright; see http://jcp.aip.org/about/rights_and_permissions

TABLE I. Electron impact cross sections (10^{-16} cm^2/sr) for excitation to the unresolved $1^3B_1 + 1^1B_1 + 1^3A_1 + 1^3A_2 + 1^1A_2 + 1^3B_2$ electronic states ($E_{loss} \sim 4.3$ eV) of pyrimidine. ICS (10^{-16} cm^2) at each energy are also reported at the base of each column. Percentage uncertainties are reported in parentheses.

	Impact energy (eV)							
Scattered	15		20		30		50	
Angle (deg.)	σ	$\Delta\sigma$	σ	$\Delta\sigma$	σ	$\Delta\sigma$	σ	$\Delta\sigma$
10							0.0221	(74)
15					0.0186	(40)		
20	0.0357	(30)	0.0148	(29)	0.0109	(60)	0.0033	(67)
30	0.0281	(26)	0.0091	(34)	0.0061	(53)	0.0031	(57)
40	0.0106	(30)	0.0076	(31)	0.0049	(41)	0.00120	(67)
50	0.0083	(26)	0.0036	(24)	0.0028	(40)	0.00125	(39)
60	0.0048	(25)	0.0037	(27)	0.0026	(29)	0.00081	(35)
70	0.0067	(28)	0.0036	(23)	0.0030	(27)	0.00081	(44)
80	0.0088	(22)	0.0043	(24)	0.0031	(27)	0.00055	(59)
90	0.0085	(27)	0.0050	(23)	0.0024	(26)	0.00064	(31)
ICS	0.165	(48)	0.098	(49)	0.057	(51)	0.025	(60)

TABLE II. Electron impact cross sections (10^{-16} cm^2/sr) for excitation to the unresolved $2^3A_1 + 1^1B_2 + 2^3A_2$ electronic states ($E_{loss} \sim 5.2$ eV) of pyrimidine. ICS (10^{-16} cm^2) at each energy are also reported at the base of each column. Percentage uncertainties are reported in parentheses.

	Impact energy (eV)							
Scattered	15		20		30		50	
Angle (deg.)	σ	$\Delta\sigma$	σ	$\Delta\sigma$	σ	$\Delta\sigma$	σ	$\Delta\sigma$
10							0.0443	(47)
15					0.0329	(30)		
20	0.0493	(32)	0.0243	(24)	0.0189	(45)	0.0106	(40)
30	0.0472	(27)	0.0203	(25)	0.0135	(28)	0.0055	(36)
40	0.0142	(29)	0.0120	(24)	0.0081	(30)	0.0022	(40)
50	0.0113	(28)	0.0060	(22)	0.0036	(37)	0.00117	(37)
60	0.0057	(33)	0.0060	(25)	0.0026	(31)	0.00092	(33)
70	0.0082	(36)	0.0041	(25)	0.0032	(25)	0.00098	(45)
80	0.0112	(22)	0.0045	(23)	0.0032	(26)	0.00071	(42)
90	0.0122	(27)	0.0056	(23)	0.0027	(24)	0.00064	(32)
ICS	0.26	(50)	0.13	(45)	0.083	(47)	0.039	(49)

TABLE III. Electron impact cross sections (10^{-16} cm^2/sr) for excitation to the unresolved $2^3B_1 + 2^1A_2 + 2^1B_1$ electronic states ($E_{loss} \sim 5.9$ eV) of pyrimidine. ICS (10^{-16} cm^2) at each energy are also reported at the base of each column. Percentage uncertainties are reported in parentheses.

	Impact energy (eV)							
Scattered	15		20		30		50	
Angle (deg.)	σ	$\Delta\sigma$	σ	$\Delta\sigma$	σ	$\Delta\sigma$	σ	$\Delta\sigma$
10							0.0234	(63)
15					0.0212	(37)		
20	0.0250	(31)	0.0140	(27)	0.0125	(55)	0.0047	(53)
30	0.0244	(29)	0.0097	(30)	0.0058	(51)	0.0029	(55)
40	0.0083	(36)	0.0071	(30)	0.0046	(42)	0.00116	(57)
50	0.0065	(29)	0.0028	(27)	0.0021	(48)	0.00082	(53)
60	0.0023	(33)	0.0025	(33)	0.0016	(38)	0.00047	(49)
70	0.0029	(31)	0.0019	(31)	0.0019	(32)	0.00050	(71)
80	0.0040	(26)	0.0019	(29)	0.0017	(37)	0.00044	(57)
90	0.0053	(29)	0.0024	(28)	0.0015	(30)	0.00040	(38)
ICS	0.106	(49)	0.061	(51)	0.047	(53)	0.019	(58)

Downloaded 01 Jan 2013 to 129.96.237.231. Redistribution subject to AIP license or copyright; see http://jcp.aip.org/about/rights_and_permissions

TABLE IV. Electron impact cross sections (10^{-16} cm^2/sr) for excitation to the unresolved $2^3B_2 + 2^1A_1 + 2^1B_2 + 3^3A_1 + 3^3B_2$ electronic states ($E_{loss} \sim 6.7$ eV) of pyrimidine. ICS (10^{-16} cm^2) at each energy are also reported at the base of each column. Percentage uncertainties are reported in parentheses.

	Impact energy (eV)							
Scattered	15		20		30		50	
Angle (deg.)	σ	$\Delta\sigma$	σ	$\Delta\sigma$	σ	$\Delta\sigma$	σ	$\Delta\sigma$
10							0.1231	(48)
15					0.0828	(25)		
20	0.0758	(33)	0.0425	(23)	0.0463	(33)	0.0280	(41)
30	0.0589	(30)	0.0333	(24)	0.0242	(28)	0.0113	(30)
40	0.0159	(29)	0.0171	(27)	0.0155	(28)	0.0049	(35)
50	0.0127	(30)	0.0078	(26)	0.0065	(34)	0.0023	(32)
60	0.0045	(36)	0.0072	(31)	0.0043	(30)	0.0015	(31)
70	0.0049	(31)	0.0045	(31)	0.0054	(26)	0.0018	(41)
80	0.0075	(27)	0.0047	(25)	0.0048	(26)	0.0011	(41)
90	0.0092	(26)	0.0068	(25)	0.0042	(25)	0.0011	(31)
ICS	0.24	(46)	0.154	(45)	0.156	(43)	0.084	(48)

TABLE V. Electron impact cross sections (10^{-16} cm^2/sr) for excitation to the unresolved $3^1A_1 + 4^1A_1 + 3^1B_2 + 3^1B_1 + 4^1B_2$ electronic states ($E_{loss} \sim 7.5$ eV) of pyrimidine. ICS (10^{-16} cm^2) at each energy are also reported at the base of each column. Percentage uncertainties are reported in parentheses.

	Impact energy (eV)							
Scattered	15		20		30		50	
Angle (deg.)	σ	$\Delta\sigma$	σ	$\Delta\sigma$	σ	$\Delta\sigma$	σ	$\Delta\sigma$
10							0.6163	(42)
15					0.3536	(22)		
20	0.2233	(36)	0.1502	(22)	0.1818	(28)	0.1256	(44)
30	0.1688	(31)	0.1170	(25)	0.0964	(22)	0.0437	(22)
40	0.0387	(27)	0.0482	(23)	0.0566	(22)	0.0205	(30)
50	0.0284	(34)	0.0264	(32)	0.0238	(26)	0.0077	(22)
60	0.0105	(39)	0.0254	(32)	0.0150	(23)	0.0063	(22)
70	0.0090	(33)	0.0142	(30)	0.0183	(22)	0.0080	(29)
80	0.0116	(30)	0.0148	(22)	0.0180	(22)	0.0050	(34)
90	0.0174	(25)	0.0259	(24)	0.0164	(21)	0.0041	(28)
ICS	0.55	(45)	0.72	(57)	0.67	(42)	0.45	(44)

TABLE VI. Electron impact cross sections (10^{-16} cm^2/sr) for excitation to unresolved Rydberg states ($E_{loss} \sim 8.3$ eV) of pyrimidine. ICS (10^{-16} cm^2) at each energy are also reported at the base of each column. Percentage uncertainties are reported in parentheses.

	Impact energy (eV)							
Scattered	15		20		30		50	
Angle (deg.)	σ	$\Delta\sigma$	σ	$\Delta\sigma$	σ	$\Delta\sigma$	σ	$\Delta\sigma$
10							0.1497	(54)
15					0.0942	(25)		
20	0.0617	(35)	0.0436	(25)	0.0527	(31)	0.0269	(45)
30	0.0497	(32)	0.0313	(29)	0.0233	(28)	0.0098	(31)
40	0.0103	(31)	0.0136	(29)	0.0153	(27)	0.0051	(33)
50	0.0091	(32)	0.0087	(30)	0.0079	(29)	0.0022	(30)
60	0.0030	(35)	0.0083	(32)	0.0055	(27)	0.0017	(28)
70	0.0028	(31)	0.0045	(34)	0.0063	(24)	0.0022	(36)
80	0.0032	(41)	0.0040	(25)	0.0061	(24)	0.0015	(44)
90	0.0038	(24)	0.0076	(25)	0.0051	(23)	0.0013	(30)
ICS	0.140	(44)	0.162	(47)	0.161	(42)	0.086	(50)

Downloaded 01 Jan 2013 to 129.96.237.231. Redistribution subject to AIP license or copyright; see http://jcp.aip.org/about/rights_and_permissions

TABLE VII. Electron impact cross sections (10^{-16} cm^2/sr) for excitation to unresolved Rydberg states (E_{loss} ~ 9.2 eV) of pyrimidine. ICS (10^{-16} cm^2) at each energy are also reported at the base of each column. Percentage uncertainties are reported in parentheses.

	Impact energy (eV)							
Scattered	15		20		30		50	
Angle (deg.)	σ	$\Delta\sigma$	σ	$\Delta\sigma$	σ	$\Delta\sigma$	σ	$\Delta\sigma$
10							0.2878	(56)
15					0.1910	(25)		
20	0.0904	(39)	0.0759	(24)	0.1160	(29)	0.0585	(54)
30	0.0757	(34)	0.0588	(25)	0.0510	(24)	0.0185	(26)
40	0.0196	(29)	0.0295	(30)	0.0324	(24)	0.0093	(38)
50	0.0197	(28)	0.0185	(24)	0.0143	(32)	0.0044	(28)
60	0.0052	(29)	0.0142	(30)	0.0111	(26)	0.0025	(27)
70	0.0057	(28)	0.0078	(26)	0.0127	(23)	0.0038	(36)
80	0.0055	(30)	0.0067	(24)	0.0113	(24)	0.0025	(35)
90	0.0081	(23)	0.0110	(25)	0.0098	(22)	0.0024	(27)
ICS	0.23	(48)	0.27	(44)	0.31	(42)	0.164	(51)

observed in the photo-absorption spectra. Finally, in Fig. 4 we present the DCS for excitations to the Rydberg states found in the energy loss features at 8.3 and 9.2 eV. All those figures are now discussed in more detail.

In Fig. 2 we present the DCSs for the energy loss features centred at E_{loss} ~ 4.3 eV and E_{loss} ~ 5.9 eV. First, at the lower incident electron energies, it is apparent that the DCS for the excitation to the unresolved $1^3B_1 + 1^1B_1 + 1^3A_1 + 1^3A_2$

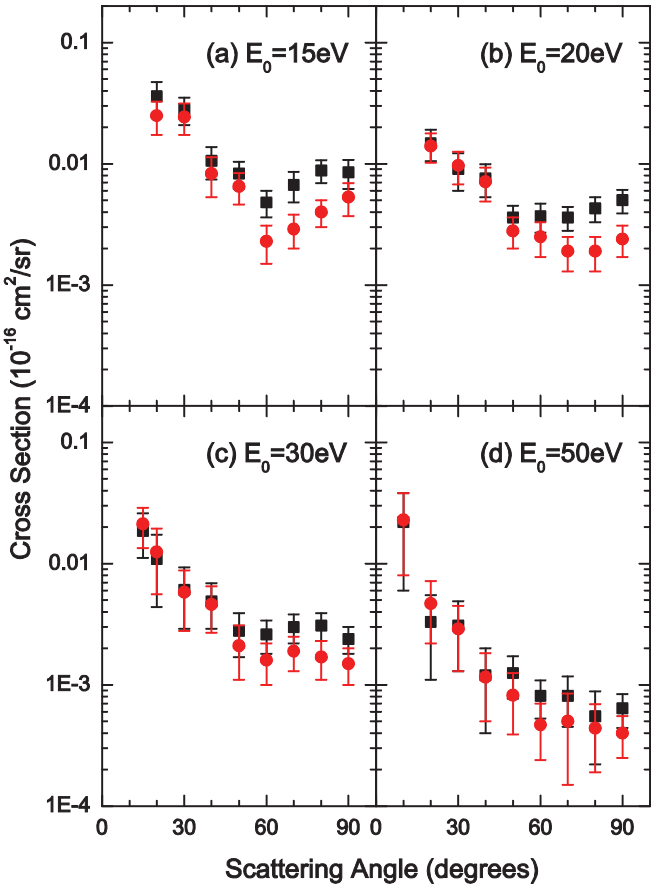

FIG. 2. Differential cross sections for the electron impact excitation of the (■) unresolved $1^3B_1 + 1^1B_1 + 1^3A_1 + 1^3A_2 + 1^1A_2 + 1^3B_2$ (E_{loss} ~ 4.3 eV) and (●) unresolved $2^3B_1 + 2^1A_2 + 2^1B_1$ (E_{loss} ~ 5.9 eV) electronic states at incident electron energies of (a) 15 eV, (b) 20 eV, (c) 30 eV, and (d) 50 eV. See text for further details.

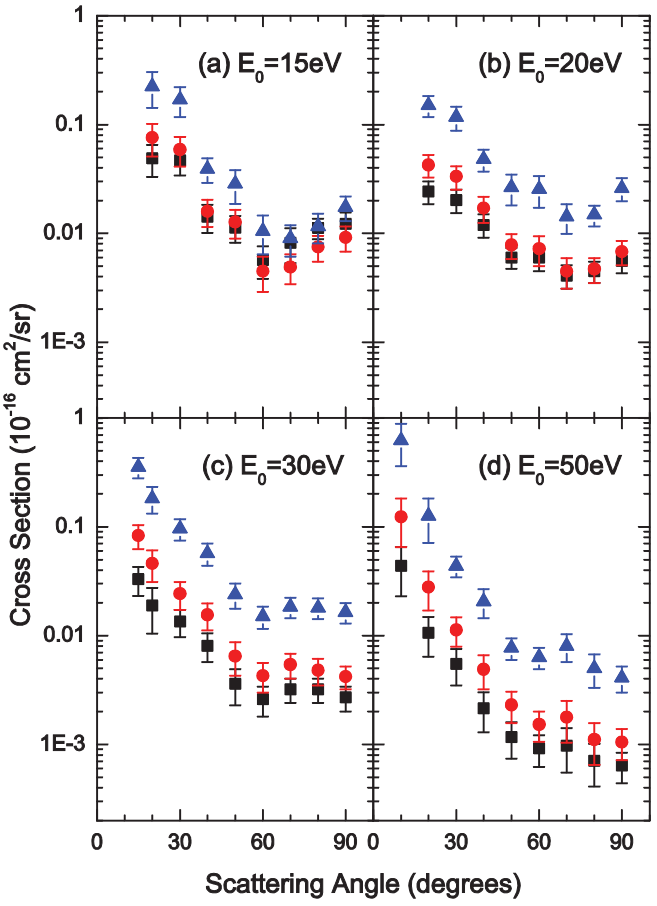

FIG. 3. Differential cross sections for the electron impact excitation of the (■) unresolved $2^3A_1 + 1^1B_2 + 2^3A_2$ (E_{loss} ~ 5.2 eV) and (●) unresolved $2^3B_2 + 2^1A_1 + 2^1B_2 + 3^3A_1 + 3^3B_2$ (E_{loss} ~ 6.7 eV), and (▲) $3^1A_1 + 4^1A_1 + 3^1B_2 + 3^1B_1 + 4^1B_2$ (E_{loss} ~ 7.5 eV) electronic states at incident electron energies of (a) 15 eV, (b) 20 eV, (c) 30 eV, and (d) 50 eV. See text for further details.

Downloaded 01 Jan 2013 to 129.96.237.231. Redistribution subject to AIP license or copyright; see http://jcp.aip.org/about/rights_and_permissions

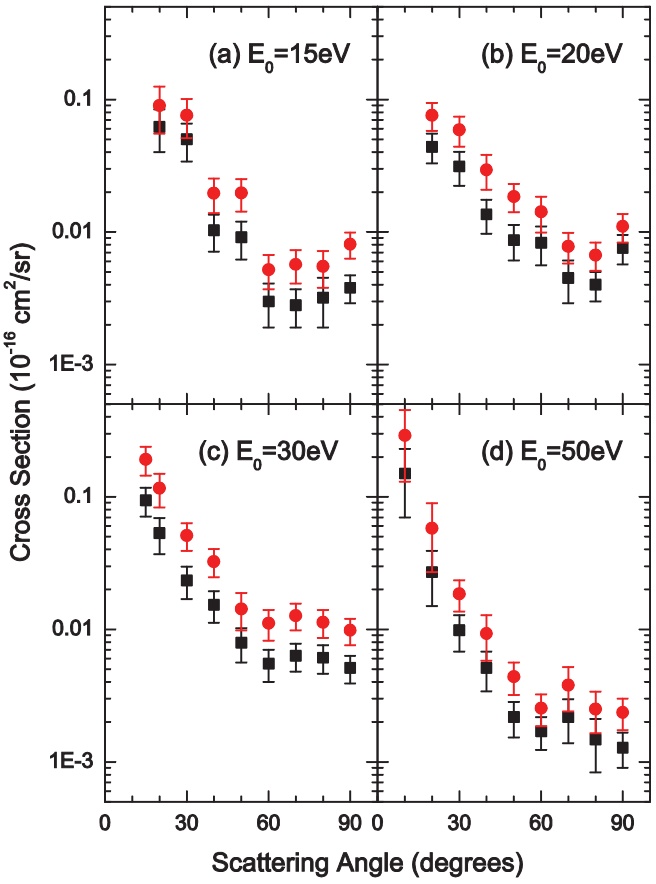

FIG. 4. Differential cross sections for the electron impact excitation of the unresolved Rydberg states at $E_{loss} \sim 8.3$ (■) and $E_{loss} \sim 9.2$ eV (●) for incident electron energies of (a) 15 eV, (b) 20 eV, (c) 30 eV, and (d) 50 eV. See text for further details.

$+ 1^1A_2 + 1^3B_2$ states ($E_{loss} \sim 4.3$ eV) gives a substantially larger intensity than that observed for excitations to the $2^3B_1 + 2^1A_2 + 2^1B_1$ electronic states ($E_{loss} \sim 5.9$ eV) at the backward scattering angles. Such backward scattering angle contributions are dominated by the electron-exchange scattering phenomena, which in particular favours singlet → triplet excitations. Note that direct scattering reduces at larger scattering angles while exchange scattering increases owing to their respective long and short range interactions.[29] Here the large number of low-lying triplet states accessible at $E_{loss} \sim 4.3$ eV increases the excitation probability relative to that found at $E_{loss} \sim 5.9$ eV. We also observe that the DCSs for both features exhibit increased intensity at the more forward scattering angles. This behaviour is characteristic of direct scattering phenomena, which we mainly attribute to contributions from weak dipole-allowed transitions to the $^1B_1$ states found in both features. This may also follow from an important contribution from spin-allowed but symmetry forbidden $^1A_1 \rightarrow {}^1A_2$ transitions, which are expected to display a weakly forward-peaked angular distribution.[30] The forward peaking observed for both energy loss features becomes more prominent as the incident electron energy increases from 15 to 50 eV. This is characteristic of a weakening of the singlet → triplet excitation processes at the higher incident electron energies where electron-exchange scattering becomes less probable.

The DCSs for the three prominent features found in the photo-absorption spectra are presented in Fig. 3. These features are attributed to excitations to the unresolved $2^3A_1 + 1^1B_2 + 2^3A_2$ ($E_{loss} \sim 5.2$ eV), $2^3B_2 + 2^1A_1 + 2^1B_2 + 3^3A_1 + 3^3B_2$ ($E_{loss} \sim 6.7$ eV) and $3^1A_1 + 4^1A_1 + 3^1B_2 + 3^1B_1 + 4^1B_2$ ($E_{loss} \sim 7.5$ eV) electronic states. In this case each unresolved excitation feature exhibits a strong DCS intensity at the forward scattering angles. This is characteristic DCS behaviour for dipole-allowed transitions.[30] Interestingly, at 15 and 20 eV incident electron energies all these DCSs still exhibit minima in their angular distributions around 60° before the DCS increase in magnitude again at the more backward scattering angles. As DCSs for spin-forbidden transitions can be found to increase as the scattering angle becomes larger,[31] or be largely isotropic (to within a factor of 2–3) (Ref. 30) over the angular distribution, we suspect that singlet → triplet transitions are also making a contribution to the DCS at these energy loss values. It is this contribution from excitations to triplet states that gives here the increased intensity at the more backward scattering angles. This behaviour was also particularly apparent in our comparative study between benzene and pyrimidine,[16] undertaken to evaluate the nature of the DCSs for π-π^* excitations. In that work we noted that important triplet state excitations of benzene, previously identified in the near-threshold electron energy loss spectra,[32] are expected to correlate to triplet states found in the energy loss feature of pyrimidine at $E_{loss} \sim 6.7$ eV. Finally, the smaller ratio of singlet to triplet states found in the feature at $E_{loss} \sim 5.2$ eV slightly alters its DCS angular distribution; being slightly less forward peaked than the other mainly dipole-allowed features, while having a larger DCS intensity at the more backward scattering angles.

Finally, the DCS for excitations to the unresolved Rydberg states at $E_{loss} \sim 8.3$ and 9.2 eV are presented in Fig. 4. In these energy loss features the bulk of the intensity is expected to arise from Rydberg like transitions converging to the $^2B_2$ ($7b_2^{-1}$), $^2B_1$ ($2b_1^{-1}$), and $^2A_1$ ($11a_1^{-1}$) ion states with ionization potentials of 9.8, 10.2, and 11.2 eV,[14] respectively. Here we observe that the Rydberg excitations in both energy loss features display the same angular behaviour in the DCS at all incident electron energies studied. In addition, at all incident electron energies the DCS for the Rydberg excitations are forward peaked. Further, any enhancement to the DCSs as the scattering angle increases is not strong here. This suggests that triplet state excitations are not significantly contributing to these energy loss features.

In summary, the present DCS measurements represent a comprehensive study of the electron-impact discrete excitation processes in pyrimidine. These DCS measurements provide important data that could be incorporated into charged-particle track simulations for elucidating the effect of radiation damage in biological systems. They are also expected to provide key insights into electron scattering phenomena from more complex biological systems. These measurements also represent important data for assessing the reliability of theoretically calculated DCSs for electron-impact excitation processes when they become available. We expect that such calculations may become available in the near future, with integral cross

Downloaded 01 Jan 2013 to 129.96.237.231. Redistribution subject to AIP license or copyright; see http://jcp.aip.org/about/rights_and_permissions

sections for electron-impact excitation processes having recently been computed for pyrimidine.[17] Finally, by comparing the angular behaviour of DCSs derived from energy loss features of unresolved transitions we have been able to identify the important scattering mechanisms that contribute at each energy loss.

V. CONCLUSION

Absolute differential cross sections for the electron-impact excitation of electronic states in pyrimidine were measured for the first time. Here DCSs were reported for six inelastic features spanning the electronic excitation processes below the first ionization potential, at incident electron energies between 15 and 50 eV and over the 10°–90° angular range. All of the measured DCSs for the inelastic features exhibited some degree of forward-peaking in their angular distribution, which was attributed to direct scattering phenomena associated with dipole-allowed excitations. At the low incident electron energies, electron-exchange scattering was found to play an important role in exciting the triplet states of pyrimidine at the more backward scattering angles. Here the number of states of a given symmetry and spin multiplicity, in an energy loss feature, was also found to influence the nature of the relevant DCS angular distribution.

These measurements also represent an important addition to the available literature on electron scattering from pyrimidine, where it is now probably conceivable to include pyrimidine as a DNA moiety in charged-particle track simulations. This represents an important step towards elucidating the effect of radiation damage on biological systems. While the present measurements do provide some key insights into the behaviour of the electron-impact excitation mechanisms in pyrimidine, theoretical calculations of the DCS are particularly desirable for gaining a more detailed analysis of the individual excitation mechanisms observed in the unresolved energy loss features.

ACKNOWLEDGMENTS

This research was supported by the ARC through its Centres of Excellence program. D.B.J. acknowledges financial support provided through an ARC Discovery Early Career Researcher Award. M.J.B. also acknowledges the University of Malaya for his "Distinguished Visiting Professorship." P.L.-V. acknowledges the PEst-OE/FIS/UI0068/2011 grant. Partial financial support from the Spanish Ministerio de Ciencia e Innovacion through Project No. FIS2009-10245 is also acknowledged. This work also forms part of the EU/ESF COST Action MP1002.

[1] I. Plante and F. A. Cucinotta, New J. Phys. **11**, 063047 (2009).
[2] B. Boudaiffa, P. Cloutier, D. Hunting, M. A. Huels, and L. Sanche, Science **287**, 1658 (2000).
[3] F. Ferreira da Silva, D. Almeida, G. Martins, A. R. Milosavljevic, B. P. Marinkovic, S. V. Hoffmann, N. J. Mason, Y. Nunes, G. Garcia, and P. Limao-Vieira, Phys. Chem. Chem. Phys. **12**, 6717 (2010).
[4] A. G. Sanz, M. C. Fuss, A. Munoz, F. Blanco, P. Limao-Vieira, M. J. Brunger, S. J. Buckman, and G. Garcia, Int. J. Radiat. Biol. **88**, 71 (2012).
[5] K. F. Ness, R. E. Robson, M. J. Brunger, and R. D. White, J. Chem. Phys. **136**, 024318 (2012).
[6] A. Munoz, F. Blanco, G. Garcia, P. A. Thorn, M. J. Brunger, J. P. Sullivan, and S. J. Buckman, Int. J. Mass Spectrom. **277**, 175 (2008).
[7] X. Pan, P. Cloutier, D. Hunting, and L. Sanche, Phys. Rev. Lett. **90**, 208102 (2003).
[8] F. Martin, P. D. Burrow, Z. L. Cai, P. Cloutier, D. Hunting, and L. Sanche, Phys. Rev. Lett. **93**, 068101 (2004).
[9] R. D. White and R. E. Robson, Phys. Rev. Lett. **102**, 230602 (2009).
[10] P. Palihawadana, J. Sullivan, M. Brunger, C. Winstead, V. McKoy, G. Garcia, F. Blanco, and S. Buckman, Phys. Rev. A **84**, 062702 (2011).
[11] J. B. Maljkovic, A. R. Milosavljevic, F. Blanco, D. Sevic, G. Garcia, and B. P. Marinkovic, Phys. Rev. A **79**, 052706 (2009).
[12] A. Zecca, L. Chiari, G. Garcia, F. Blanco, E. Trainotti, and M. J. Brunger, J. Phys. B **43**, 215204 (2010).
[13] J. D. Builth-Williams, S. M. Bellm, D. B. Jones, H. Chaluvadi, D. H. Madison, C. G. Ning, B. Lohmann, and M. J. Brunger, J. Chem. Phys. **136**, 024304 (2012).
[14] C. G. Ning, K. Liu, Z. H. Luo, S. F. Zhang, and J. K. Deng, Chem. Phys. Lett. **476**, 157 (2009).
[15] P. L. Levesque, M. Michaud, and L. Sanche, J. Chem. Phys. **122**, 094701 (2005).
[16] D. B. Jones, S. M. Bellm, P. Limão-Vieira, and M. J. Brunger, Chem. Phys. Lett. **535**, 30 (2012).
[17] Z. Masin, J. D. Gorfinkiel, D. B. Jones, S. M. Bellm, and M. J. Brunger, J. Chem. Phys. **136**, 144310 (2012).
[18] G. L. Blackman, R. D. Brown, and F. R. Burden, J. Mol. Spectrosc. **35**, 444 (1970).
[19] Z. Kisiel, L. Pszczolkowski, J. C. Lopez, J. L. Alonso, A. Maris, and W. Caminati, J. Mol. Spectrosc. **195**, 332 (1999).
[20] P. Y. Chen and R. A. Holroyd, J. Phys. Chem. **100**, 4491 (1996).
[21] A. Bolovinos, P. Tsekeris, J. Philis, E. Pantos, and G. Andritsopoulos, J. Mol. Spectrosc. **103**, 240 (1984).
[22] M. Stener, P. Decleva, D. M. P. Holland, and D. A. Shaw, J. Phys. B **44**, 075203 (2011).
[23] M. H. Palmer, I. C. Walker, M. F. Guest, and A. Hopkirk, Chem. Phys. **147**, 19 (1990).
[24] G. Fischer, Z.-L. Cai, J. R. Reimers, and P. Wormell, J. Phys. Chem. A **107**, 3093 (2003).
[25] Y. J. Li, J. Wan, and X. Xu, J. Comput. Chem. **28**, 1658 (2007).
[26] M. Nooijen, Spectrochim. Acta, Part A **55**, 539 (1999).
[27] M. J. Brunger and P. J. O. Teubner, Phys. Rev. A **41**, 1413 (1990).
[28] M. Allan, J. Phys. B **38**, 3655 (2005).
[29] A. Kuppermann, J. K. Rice, and S. Trajmar, J. Phys. Chem. **72**, 3894 (1968).
[30] F. A. Gianturco and A. Jain, Phys. Rep. **143**, 347 (1986).
[31] T. P. T. Do, K. L. Nixon, M. Fuss, G. Garcia, F. Blanco, and M. J. Brunger, J. Chem. Phys. **136**, 184313 (2012).
[32] M. Allan, J. Electron Spectrosc. Relat. Phenom. **48**, 219 (1989).

Downloaded 01 Jan 2013 to 129.96.237.231. Redistribution subject to AIP license or copyright; see http://jcp.aip.org/about/rights_and_permissions